Why does the Kuroshio northeast of Taiwan shift shelfward in winter?

Lie-Yauw Oey · Yi-Chia Hsin · Chau-Ron Wu

Abstract Observations indicate that off the northeastern coast of Taiwan a branch of the Kuroshio intrudes farther northward in winter onto the shelf of the East China Sea. We demonstrate that this seasonal shift can be explained solely by winter cooling. Cooling produces downslope flux of dense shelf water that is compensated by shelfward intrusion. Parabathic isopycnals steepen eastward in winter and couple with the cross-shelf topographic slope (the "JEBAR" effect) to balance the enhanced intrusion. The downslope flow also increases vortex stretching and decreases the thickness of the inertial boundary layer, resulting in a Kuroshio that shifts closer to the shelf break.

Keywords Kuroshio migration · Model simulation · Cooling · JEBAR

1 Introduction

Off the northeastern coast of Taiwan, the Kuroshio collides with the (nearly) zonal-running continental shelf break of the East China Sea (Fig. 1). The current turns sharply east-northeastward to continue along the shelf break, approxi-

mately the 200-m isobath. Near the turning region, observations indicate vigorous interaction of the Kuroshio and the East China Sea (shelf) waters (Tang et al. 2000; Liang et al. 2003). The interaction consists of upwelling and cross-shelf break water-mass exchange that can have important implications for nutrient and other bio-chemical fluxes and distributions (Liu et al. 1992; Chen 1996; Gong et al. 1997). Cross-shelf mass exchange depends in part on the position of the Kuroshio relative to the shelf. Near the surface, approximately in the upper 100 m, the Kuroshio tends to be farther away from the shelf in summer than in winter (Nitani 1972; Sun 1987; Tang et al. 2000; Liang et al. 2003). This seasonal migration may be seen in Sun's (1987) summary plot of the surface axis of the Kuroshio based on 25-year geomagnetic electrokinetograph data (Sun's plot is also shown in Fig. 2 of Tang and Yang 1993). The (summer) offshore shift is often accompanied by the appearance of cyclonic recirculation over the outer shelf (Wu et al. 2008).

Theoretical explanations of why some fluid can bifurcate onto the shallow shelf as the Kuroshio negotiates the sharp bend of the East China Sea continental shelf break are given in Stern and Austin (1995; see also Hsueh et al. 1992; Carnevale et al. 1999). Although we are not concerned with the bifurcation dynamics, Stern and Austin's (1995) analytical model in particular have important consequences to the seasonal shift. We will use their ideas and vorticity analyses to offer an explanation of the seasonal change in the strength of the bifurcation which will simply be referred to as "seasonal migration." The focus is near the surface where most of the observations exist.

Several factors may influence the seasonal migration of the Kuroshio. Models forced by winds (e.g., Chao 1991 and Chen et al. 1996) suggest that the seasonal migration may be related to the monsoonal wind variations: onshore (offshore) Ekman flux in winter (summer) due to the wind

L.-Y. Oey
Program in Atmospheric and Oceanic Sciences,
Princeton University,
Princeton, USA

Y.-C. Hsin · C.-R. Wu (✉)
Department of Earth Sciences,
National Taiwan Normal University,
88, Section 4 Ting-Chou Road,
Taipei 11677, Taiwan
e-mail: cwu@ntnu.edu.tw
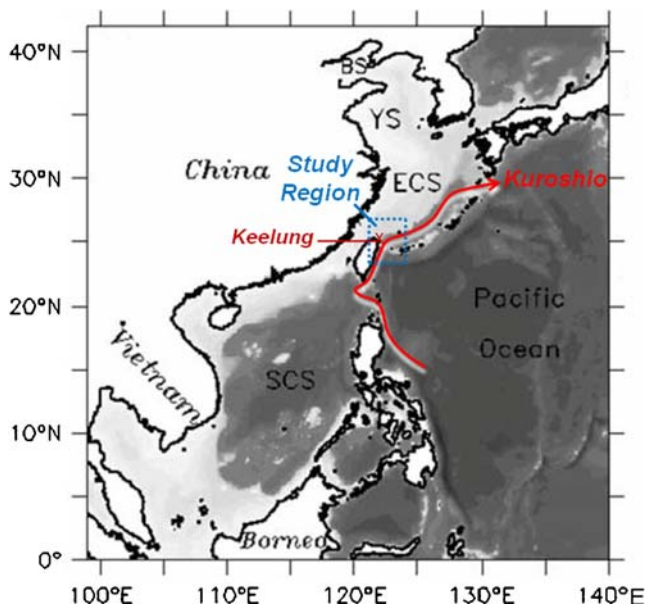
Fig. 1 Topography of the study region (*light shades* are shelves where depths are shallower than 200 m) and a schematic sketch of the Kuroshio (*in red*) showing the current's sharp right-hand turn as it approaches the continental shelf break of the East China Sea (ECS) off the northeastern coast of Taiwan. *SCS* South China Sea, *YS* Yellow Sea

from the northeast (southwest) may force the surface waters of the Kuroshio to migrate onshore (offshore). There is observational evidence that the onshore migration of the Kuroshio in fall and winter is not solely related to wind (Tang and Yang 1993, and Chuang and Liang 1994). These authors found that Acoustic Doppler Current Profilers (ADCPs) deployed over the upper slope (where water depths≈300 m) indicate currents that are not well correlated with the local wind: on-shelf intrusions of Kuroshio waters occurred long after (more than 1 month) the fall-winter monsoonal wind from the northeast had begun. Given a typical downwelling (or upwelling) response time of about 5~10 days (e.g., Allen and Newberger 1996), the lag time of more than 1 month makes it unlikely that the observed on-shelf intrusion was caused by winds. Observations also show that the intrusions were prolonged, about 1.5 months or longer through the end of the observations. There was also one intrusion event of approximately 1 month (in August 1992) following a period of summertime wind from the southwest; the event occurred during a period when five typhoons passed over the Kuroshio and further offshore (Chuang and Liang 1994). Tang and Yang (1993) found that sea level data recorded at Keelung at the northern coast of Taiwan show a summertime high and wintertime low which by geostrophy probably reflects the southward retreat and northward intrusion, respectively, of the Kuroshio. The authors found that the northward transport computed from the ADCP measurements and Keelung sea level was

visually correlated during the (short) observation period. They hypothesized that the intrusion may be related to some "non-local factors."

The idea of a non-local forcing, perhaps as it relates to the large-scale seasonal shift in the wind pattern over the Pacific, hence also to the seasonal changes in the Kuroshio transport upstream (which is probably what Tang and Yang had in mind), may be worth pursuing in the future. At present, the relevant observations are incomplete, so that it is not entirely clear how such forcing may give rise to the seasonal intrusion of the Kuroshio. For example, although the Kuroshio transport off the eastern coast of Philippines shows a seasonal variation (strong in spring, weak in fall; Wyrtki 1961; Qu et al. 1998), Johns et al. (2001) observed no clear seasonal trend in the Kuroshio transport off the eastern coast of Taiwan at approximately 24.5°N. Transport variations are dominated instead by propagating eddies (from the open Pacific) that impinge upon the eastern slope of Taiwan (Zhang et al. 2001). Effects of these eddies on the dynamics of intrusion are not trivial.

Chuang and Liang (1994) offered another explanation of why preferential northward intrusion of the Kuroshio may occur in fall and winter. The authors noted that while northward intrusion was not observed shortly (i.e., a few days) after the monsoonal wind turned northeasterly (described above), as would be expected from wind-driven Ekman dynamics, it coincided well with the arrival of cold air outbreaks in fall; moreover, onshore intrusions continued through winter. The authors proposed that surface cooling produces dense water over the shelf, which spills off-shelf over the slope and triggers on-shelf intrusion of the warmer Kuroshio water near the surface. In summer, the shelf water warms and intrusion ceases. The authors did not explain the relevant dynamics.

Numerical model simulations using realistic topography and forcing also indicate that the cross-slope (intrusive) transport has a seasonal signal that is independent of the wind. Here, we describe two of these simulations. The first is the model simulation of the Kuroshio and the East China Sea by Guo et al. (2006). The model (the Princeton Ocean Model or POM, Mellor 2002; with 1/18° horizontal resolution and 21 terrain-following sigma levels) is forced by weekly wind stress and sea surface temperature (SST) data, and also by monthly heat flux and sea-surface salinity data. An analysis of terms in the vorticity of the vertically averaged momentum equations shows that along the shelf break (defined as the 200-m isobath), the Joint Effect of Baroclinicity and Relief (JEBAR, Huthnance 1984; see also "Section 2") term balances the advection of the geostrophic potential vorticity ("f/H" where H is the water depth and f is the Coriolis parameter) term, with the wind stress term (vorticity produced by Ekman flow crossing isobaths and by wind stress curl) being almost an order of magnitude

weaker (see their Fig. 21). Guo et al. (2006) show that, since JEBAR comprises the vector-product of the cross-slope topography gradient and along isobath gradient of the potential energy of the water column, a density gradient along the slope appears to be consistent with the (simulated) intrusive transport.

The second model simulation is by Wu et al. (2008). The simulation used POM at $1/20^\mathrm{o}$ horizontal resolution and 26-sigma levels, and specifically targeted the region northeast of Taiwan. Six-hourly QSCAT/NCEP blended wind and weekly Advanced Very High Resolution Radiometer SST were used from 1999 through 2003. The authors found that (model) cyclonic eddies tend to develop more frequently (three times more often) in summer than in winter. Mode-1 Empirical Orthogonal Function shows two peaks: one off the northeastern coast of Taiwan over the outer shelf and the other one to the southeast in the Kuroshio (see their Fig. 4). The two (in-phase) peaks indicate that cyclonic eddies are generally associated with the offshore migrations of the Kuroshio. These migrations were not found to be related to the wind forcing.

In this work, we explore the possibility that cooling alone can cause the seasonal migration of the Kuroshio, and we seek to explain the process in a model that isolates the effects of cooling. Section 2 sketches the process we have in mind, using the planetary geostrophic equations (Salmon 1992) and Stern and Austin's (1995) model as the bases for our argument. In Section 3, we use a general circulation model (POM) to run experiments with idealized forcing that isolates the Kuroshio migration due to the seasonal cooling. Section 4 describes our results. We demonstrate the robustness of our results by not focusing on one or two specific intrusion events, but rather on an aggregate of them over a long period (10 years), so that the seasonal signal may be extracted. We show that wintertime spillage of dense shelf waters leads to vortex stretching and enhanced compensating (shelfward) transport. The enhanced intrusion in winter is moreover consistent with a stronger coupling of parabathic density gradients caused by cooling with the cross-shelf topographic slope (the "JEBAR" effect). The paper ends with summary and discussion in Section 5.

2 Processes

The northward-flowing Kuroshio turns sharply eastward for some distance, about 200 km and more, along the nearly zonal running isobaths at approximately the 25.5^oN latitude off the northeastern coast of Taiwan. Winter cooling is strongest near the coast (Taiwan) and it weakens along the (approximately) eastward current. Figure 2 gives a schematic illustration of the processes involved. The x, y, and z are positive eastward, northward, and upward, respectively.

Figure 2a shows an idealized Kuroshio along the zonal running isobaths and indicates also cooling over the western portion of the current. Figure 2b shows more details. The preferential cooling near Taiwan decreases the upper layer which deepens eastward (i.e., $h_{d1} > h_1$ in the figure). This produces parabathic (i.e., along isobath) pressure gradient which acts in conjunction with the topographic gradient to balance diabathic (across isobaths) flows. This so-called "JEBAR" effect and its generation by cooling may be understood from the following equations that relate the upper layer depth $h_1(x, y, t)$ and the total (i.e., depth integrated) transport stream function $\psi(x, y, t)$ (Salmon, 1992; see Appendix Eqs. 8 and 12):

$$\mathrm{D}\psi(h_1)/\mathrm{D}t = (h_1/H)u_{\mathrm{Ib}}.\nabla H + \nabla.\left(rR_o{}^2\nabla h_1\right) + Q \quad (1)$$

$$U.\nabla(f/H) = +g'k\left[\left(\nabla h_1{}^2/2\right) \times \nabla(1/H)\right]$$
$$- \nabla.\left[(r/H)\nabla\psi\right] \quad (2)$$

In Eq. 1,

$$\mathrm{D}\psi/\mathrm{D}t = \partial/\partial t + \left(-\psi_y/H\right)(\partial/\partial x) + (\psi_x/H)(\partial/\partial y) \quad (3)$$

denotes the rate of change following a fluid parcel moving with the depth-averaged flow (see LHS of Eq. 8), and the u_{Ib} is a horizontal vector whose components are the two terms in the square brackets on the RHS of Eq. 8. It is in fact the lower layer velocity without the Ekman contributions, as an inspection of Eqs. 7c, 7d) readily shows. The first term on the RHS of Eq. 1 therefore represents the rate of change on h_1 as the bottom velocity flows over topography. The term is negative tending to decrease h_1 for flow going "uphill" (i.e., upwelling; because u_{Ib} and ∇H then point in opposite directions) and it is positive for flow going downhill. The second term on the RHS of Eq. 1 is frictional contribution to the change in the upper layer depth. Friction tends to flatten anomaly (so that currents are reduced), so the term is negative for a local maximum in h_1 ($\nabla^2 h_1 < 0$, take $rR_o{}^2 \approx$ constant) and positive for a local minimum. The last term on the RHS of Eq. 1 represents cooling (heating) for $Q < 0$ ($Q > 0$) which tends to decrease (increase) h_1.

The first term on the RHS of Eq. 2 is the JEBAR term; it is nil if topographic contours are parallel to the h_1 contours, i.e., if there is no variation in layer depth (or density in a continuously stratified model) along isobaths. In this case, since friction (second term on the RHS of Eq. 2) is small except near boundary layers, Eq. 2 reduces to $U.\nabla(f/H)$ and flow is along the (f/H) contours or is along isobaths since $f \approx$ constant for the small region being considered. Diabathic

Fig. 2 A schematic illustration of the hypothesized processes involved in producing the on-shelf intrusion of the Kuroshio as a result of differential cooling off the northeastern coast of Taiwan. See text for details
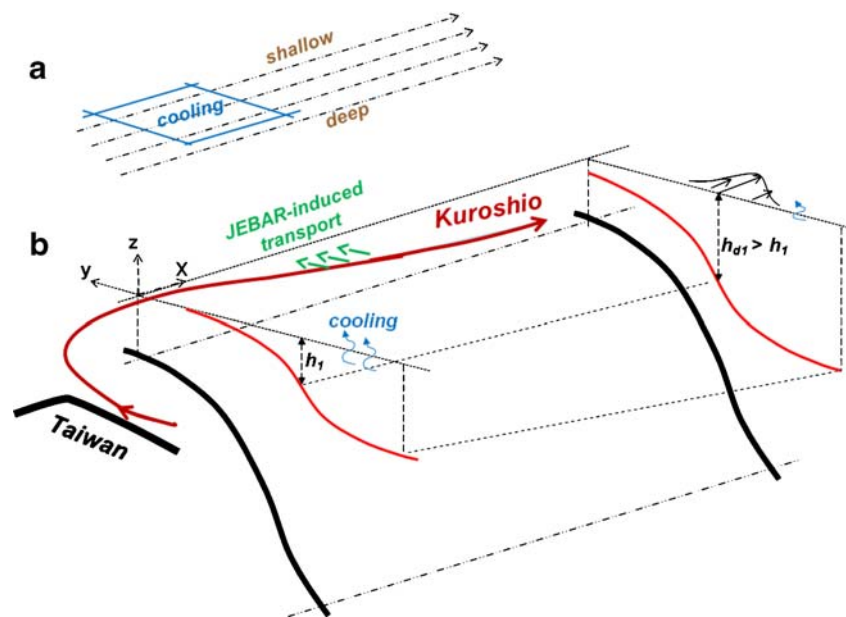
(i.e., cross-isobath) flows are produced whenever there is friction and/or if this is again assumed small, whenever isopycnals (i.e., contours of h_1^2) cross-isobaths at a non-zero (or non-π) angle. The cross-flow is towards shallower (deeper) water if the direction of steepest isopycnal ascend ∇h_1 (i.e., to the warm side) is to the right (left) of the direction of steepest topographic ascend ∇H^{-1} (i.e., to the shallow side). By right (left) we mean a spanning angle of 0 to π between the two vectors. In our problem of differential (i.e., zonally inhomogeneous) cooling during fall and winter over the western portion of the Kuroshio (Fig. 2), Q is <0 in the west and it is ≈0 towards the east. The tendency is then to induce a positive $\partial h_1/\partial x$, and to tilt eastward a ∇h_1 vector that is initially aligned with ∇H^{-1} (i.e., northward). Therefore, $\nabla h_1^2 \times \nabla H^{-1} > 0$, and the cross-flow is on-shelf. In summer, $\partial h_1/\partial x$ and the cross-flow weaken, and the current tends to follow more closely the bottom topography towards the east.

Northeast of Taiwan, because of the presence of a western boundary current at a sharp bathymetric bend, parabathic (west to east) density gradients exist irrespective of the season. Differential cooling described above therefore enhances the JEBAR effect in winter. However, JEBAR contributes to the vorticity balance; it depends on the flow field and cannot by itself be used to explain the flow. Stern and Austin (1995) suggest that, as a portion of the Kuroshio intrudes onto the East China Sea shelf, compensating outflows cross the shelf break and are then entrained by the Kuroshio. Since diabathic intrusion occurs irrespective of the season, these outflows exist in both summer and winter. However, winter cooling produces dense shelf waters which spill over the shelf break and therefore potentially can increase the amount

of entrainment into the Kuroshio. The increased entrainment also enhances the Kuroshio intrusion. Moreover, entrainment involves downslope vortex stretching which provides the cyclonic vorticity required to maintain the western boundary current in an "inertial boundary layer" (in place of a vorticity diffusion process at a no-slip wall; Stern and Austin 1995). We hypothesize that vortex stretching is enhanced by cooled dense water spillage onto the deeper slope, because the downwelling velocity is then correspondingly stronger. The increased vortex stretching in winter would then enable the same cyclonic vorticity to be produced over a shorter cross-slope distance, resulting in a thinner inertial boundary layer, and a Kuroshio that shifts closer to the shelf break.

These ideas form the basis of our hypothesis that cooling alone explains the seasonal migration of the Kuroshio off the northeastern coast of Taiwan. In the following section, a numerical model is designed to test this hypothesis.

3 The numerical model

The POM (Mellor 2002) is applied in a rectangular ocean of south-north length L=500 km and west-east length = 950 km (Fig. 3) on a β-plane $\left(\beta = 2 \times 10^{-11} m^{-1} s^{-1}\right)$. The topography consists of a rectangular land region representing Taiwan in the southwest and a quarter-pie shape East China Sea slope and shelf in the northwest (Fig. 3). The shelf's depth increases from 25 m at the northwest corner to 100 m offshore, and the steep slope varies from 100 to 1,000 m over a width of about 50 km; the deep ocean is then set constant at 1,000 m. A western
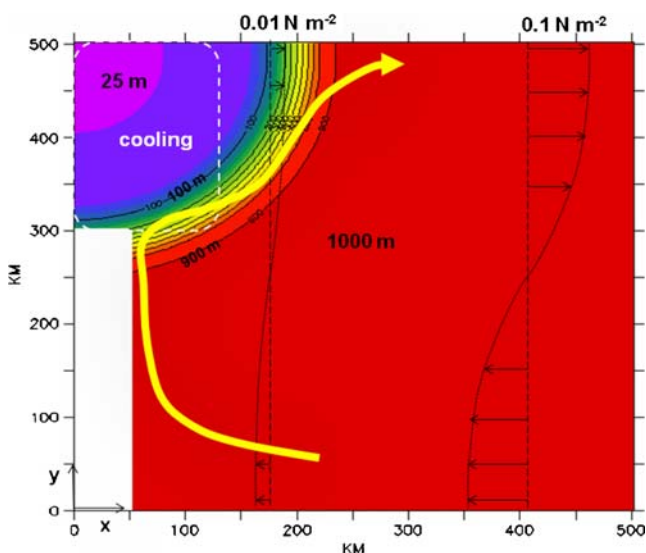
Fig. 3 The model domain and schematic sketches of the wind and heat flux forcing. The entire meridional region is shown, but only the western half of the model domain is shown. See text for other details

boundary current representing the Kuroshio is spun up by specifying a zonal wind stress

$$\rho_0 \tau^x = -0.1 \times \cos[\pi y / L] \text{Nm}^{-2}, \quad (4)$$

where, ρ_o is sea water density and τ^x is the zonal kinematic wind stress; this wind stress (i.e., Eq. 4) is tapered to zero near the western boundary (Fig. 3). The 'tapering' eliminates Ekman convergences (divergences) that can complicate the interpretations of the modeled currents caused by cooling in the region of interest. The resulting Sverdrup transport $= \int curl_z(\tau^o)/\beta \, dx$, being the kinematic wind stress vector, is approximately *24* Sv (*1* Sv$=10^6 m^3$ s^{-1}), a little larger than (by about *2~3* Sv) the observed estimates by Johns et al. (2001) off the eastern coast of Taiwan. A seasonal heat flux (positive upward, i.e., ocean loses heat) is specified as the surface boundary condition for the potential temperature equation:

$$(K_H \partial T / \partial z)|_{z=0} = -10^{-4} \sin(2\pi t / 360) \, Km/s, \quad (5)$$

where, K_H is an eddy diffusivity (m^2/s), T the potential temperature (K), and t the time in days (360 days = 1 year). The magnitude ($10^{-4} K$ m/s) gives a maximum heating and cooling of approximately ±400 W/m^2. The heating months are taken as from May 1 (zero heating) through August 1 (maximum heating) and November 1 (zero heating), and the cooling months then follow through February 1 (maximum cooling) and back to May again. To simulate the zonally inhomogeneous heat flux, Eq. 5 is tapered for winter months to zero (tanh function) eastward over a distance of approximately 150 km. Figure 4 shows the 1°×

1° ECMWF (European Centre for Medium-range Weather Forecasts) heat flux data. Off the eastern coast of Taiwan, the annual mean shown in Fig. 4 is dominated by fall-winter's (September through March) large heat loss near Taiwan and less heat loss further east, and the spatially nearly uniform heating (of small magnitude) in summer has little effects on this (spatially) inhomogeneous heat loss pattern.

The Princeton Ocean Model solves the primitive equations with hydrostatic and Boussinesq approximations on the Arakawa C-grid, and sigma (terrain following) grid in the vertical. Leap frog time-stepping is used with Asselin filter to reduce the computational mode. There are 50 equal-spaced sigma levels in the vertical. Tests on the sensitivity of the solution on model horizontal grid sizes were carried out for a 3-year simulation, with $\Delta x = \Delta y = 10$, 5, and 2.5 km. The solutions for 5 and 2.5 km are very similar while those for 10 and 5 km show significant differences. The $\Delta x = \Delta y = 5$ km grid is then chosen for extended (10 years) integration and also for more detailed analyses. The vertical eddy viscosity and diffusivity are obtained using the Mellor-Yamada turbulence closure scheme (default in POM, Mellor 2002). The horizontal viscosity is modeled using the Smagorinsky's (1963) shear-dependent formula with constant = 0.1, and the corresponding diffusivity is set ten times smaller. To reduce the so-called sigma pressure gradient errors (PGE) over steep topography (Mellor et al. 1998), a mean density $\rho_o(z)$ (see below) that varies in z only is subtracted before the baroclinic pressure gradients are calculated. Moreover, a fourth-order compact differencing is used to compute these gradients (Orszag, 1971). Tests with the seamount problem (Bernsten and Oey 2010) show that the fourth-order scheme gives PGE's of O(0.1 cm s^{-1}) for density perturbations ρ'/ρ_o of O(10^{-3}); these are an order of magnitude smaller than the errors of the standard second-order scheme.

The model is integrated from a rest state for 10 years with the surface momentum and heat fluxes as specified
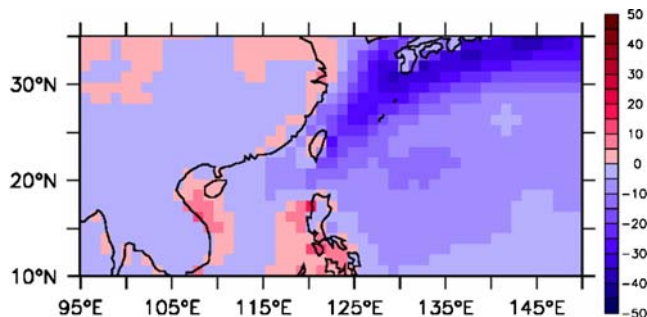
Fig. 4 Annual mean surface heat flux from 1°×1° ECMWF analysis for the period 1993 through 2001. This shows more heat loss off the northeastern coast of Taiwan than further offshore

above. The initial temperature field is a function of z only given by:

$$T_o(z) = 5 + 20 \exp(z/300), {}^{\circ}C \qquad (6)$$

For the present low (horizontal) viscosity run, the solution is unsteady and nonlinear with eddies (and Rossby waves) impinging on the western boundary current from the east (results not shown). A statistical equilibrium state is reached in 5~6 years when the domain-integrated kinetic energy has reached a quasi-steady state (oscillating about a nearly constant value). The last 4 years (7~10 years) of the model results are used for analyses.

To calculate the JEBAR term, we use the following equation to diagnose the various terms in the vorticity of the depth-averaged currents:

$$\partial \zeta_a / \partial t + (\mathrm{H}u_a).\nabla(f/H) = J(\chi, H^{-1}) + \nabla$$
$$\times [(\tau^o - \tau_b)/H] - \nabla$$
$$\times (A/H) \qquad (7)$$

where, $\zeta_a = \nabla_z \times u_a$ is the vertical component of the curl of the depth-averaged velocity $u_a = (u_a, v_a), \chi = \int_{-H}^{0} z b dz', b = g\rho/\rho_o, \tau^o$ and τ_b are the (kinematic) wind and bottom stresses, respectively, and A lumps together the horizontal advection and diffusion. The first term on the RHS of Eq. 7, $J(\chi, H^{-1})$, is the JEBAR term whose counterpart in the two-layer model is the first term on the RHS of Eq. 2. The second term on the LHS of Eq. 7, $(\mathrm{H}u_a).\nabla(f/H)$, is equivalent to the LHS of Eq. 2—it represents the advection of the geostrophic potential vorticity f/H, and is positive for on-shelf flow across isobaths.

Prior to presenting the results, we remark that since the wind is tapered, wind stress is zero over the cooled shelf region and remains very weak offshore (≈ 0.01 N m^{-2} at $x \approx$ 200 km; see Fig. 1). Vertical mixing and motion produced by cooling will be seen to be the prominent response that dynamically distinguishes winter and summer.

4 Results

Observations (see introduction) indicate that the on-shelf intrusion of the Kuroshio is confined to the surface. Figure 5 compares summer and winter sea-surface heights (SSH) and currents. Summer is defined from May through October when the modeled ocean gains heat through the specified surface heat flux (Eq. 5), and winter is from November through April when there is a surface heat loss. This is clearly a simplistic view of the effect of air-sea exchange process but would suffice for the present purpose of demonstrating the effects of surface cooling on the near-surface path of the Kuroshio. The summer solution consists of a very weak coastal current that flows along the northern shelf of Taiwan and then continues along the western boundary of the shelf. The main portion of the surface Kuroshio turns east-northeastward following the continental slope's isobaths. There is off-slope flow (i.e., across the 100-m isobath) from the shallow shelf that feeds into the cyclonic side of the Kuroshio along the slope. This near-surface off-slope flow is particularly clear in the summer. In winter, SSH over the shelf is approximately 0.1 m lower. The SSH=−0.15-m contour shows that a surface branch of the Kuroshio intrudes on-shelf and makes an anticyclonic (Ω shape) turn over the outer shelf before rejoining the main Kuroshio; a cyclone (SSH=−0.25-m contour) is formed further downstream on the outer shelf. The off-slope flow now is mainly in the narrow region between the anticyclone and cyclone, and it feeds a much narrower (by about

Fig. 5 Surface currents (blue vectors) on color sea-surface height (SSH) maps. Panel a is summer (May-Oct) and b is winter (Nov-Apr). White contours indicate SSH=−0.25 (which exists in winter only), −0.15 and +0.15 m, dash is negative and solid is positive. Dotted lines are Kuroshio paths in winter (brown) and summer (yellow)—see text. Black dotted contours are 100, 500, and 900-m isobaths
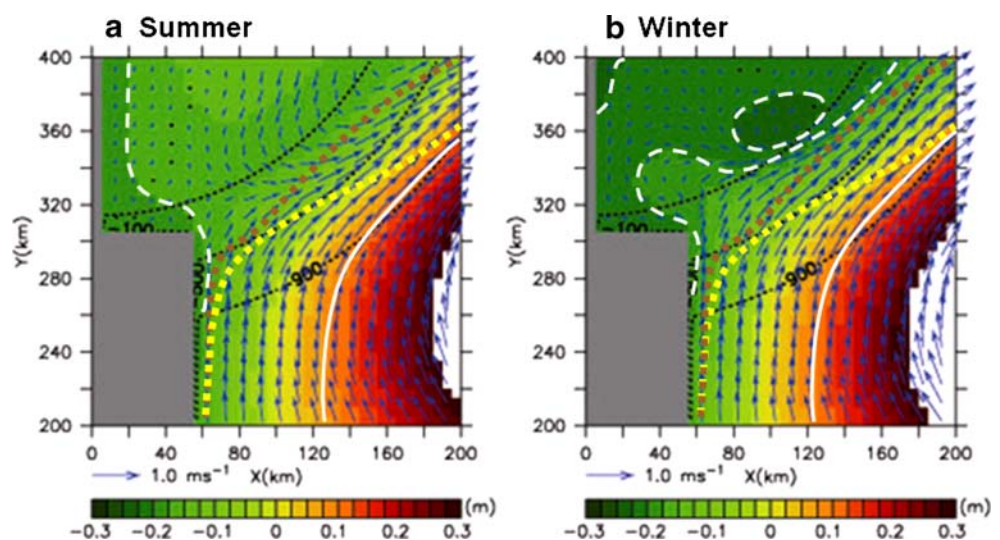
20~40 km than the summer case) cyclonic region of the Kuroshio. The Kuroshio axes in both seasons are also plotted in Fig. 5. The axis is defined as the path of local maxima of speed at $z=-50$ m along a cross-slope line drawn seaward normal to isobaths from the coast or shallow shelf; the relative vorticity is positive inshore and negative offshore of the maximum. Both axes are close to each other for $x<$ 100 km but deviate thereafter, beyond the 500-m isobaths. The summer axis veers offshore from the 500-m isobaths while the winter axis shifts inshore, coming close to the shelf break. It is clear that in winter, the Kuroshio moves closer to the outer shelf than in summer.

Figure 6 shows depth and along-isobath sectional contours of along-section velocity (U; i.e., parabathic), across-section velocity (V; i.e., diabathic), temperature (T), and vertical velocity (W) along various isobaths. For temperature, the largest difference between summer and winter is in the upper 100 m approximately above the 16°C-contour. Near Taiwan, winter stratification is weak caused by vertical mixing due to cooling. The presence of a western boundary current means that isotherms deepen away from the coast along isobaths, and one expects the JEBAR term to play a role irrespective of seasons. However, because of cooling, the isotherm-deepening is steeper in winter (see the 17°C isotherm), from the coast to approximately 80 km offshore where much of the increased shelfward intrusion of the Kuroshio occurs. This enhanced intrusion is seen in the V-contours which off Taiwan show increased maximum V of about 30% in winter than in summer (e.g., along the 300-m isobath). (Note that because isobaths do not intersect Taiwan at right angle, the V is not parallel to the coast). The increased V exists at all depths but is most apparent in the upper layer (~100 m). Across the 100 m, the diabathic offshelf flow ($V<0$) in winter shows a narrow core (at x≈100 km) with speeds exceeding -0.1 m s^{-1}, and extends from surface to bottom. In summer, the corresponding offshelf flow is weaker and wider. The Vs are similar along other (deeper) isobaths except that offshelf flows are stronger in winter. These across-isobath flow structures are consistent with the "bowl-shape" isotherms by thermal wind. The W-contours show upwelling (up to +50 m day^{-1} at 200-m isobath) off Taiwan and downwelling in the region of offshelf flow. The winter downwelling is stronger and more intensified than summer especially near the bottom. Across the 100-m isobath, downwelling extends to the bottom in winter (W≈−40 m day^{-1}) and advects cold (high potential vorticity) shelf water down the slope. Stretching by downslope flow results in up-doming of the isotherms (near x≈120 km) which are more intense in winter than summer, as is clearly seen in the T-contours along the 100-m isobath. Finally, the along isobath flow (U) accelerates away from the coast, becoming strong before it weakens as the isobaths curve northward. The latter weakening is because the model Kuroshio tends to veer

offshore away from the northward-curving isobaths (Fig. 5); we will see that the veering is consistent with a locally negative JEBAR term.

We hypothesized previously that winter-cooled shelf water sinks downslope and contributes to the thinner inertial boundary layer at the inshore portion of the model Kuroshio; a thin boundary layer means a shoreward shift in the Kuroshio axis in winter (Fig. 5). Since the model is hydrostatic, downwelling is by ageostrophic adjustments by vigorous winter mixing over the outer shelf. In a cross-slope vertical plane, a front is formed separating winter-cooled well-mixed shelf water from the warm Kuroshio water (plots not shown). Downwelled shelf waters leak off-slope from the foot of the front, and is entrained by the Kuroshio. This off-slope flux is compensated by onshore influx which can be either from Kuroshio intrusion across the southern portion of the shelf (off the northeastern coast of Taiwan), or/and from westward flow across the eastern portion of the shelf (Fig. 3). Contribution from the east is nearly zero (not shown), so that most of the compensating shelfward influx comes from the Kuroshio intrusion. Figure 7 compares the summer and winter temperature contours at $z=-50$ m, and Fig. 8 the vertical velocity W at $z=-30$ m (this depth is chosen so one can see the wide shelf; the W's at deeper depths are stronger). It is clear from Fig. 7 that cold water exists in winter over the outer shelf from x≈65 to 130 km, and the region of cold waters is associated with off-slope and downwelling currents (Fig. 8). Downwelling and off-slope flows also exist in summer, but they are weaker.

We examine how downslope volume flux compares with the intrusive flux due to the Kuroshio off the northeastern coast of Taiwan. We compute transports across three sections formed by the 200 and 100-m isobaths and also by a cross-shelf section between the 100 and 200-m isobaths. These sections are shown in the left inset of Fig. 9. Figure 9a shows transport across the three indicated sections for the four-year analysis period. (Running averages were applied to these and below time-series to remove fluctuations caused by westward-propagating waves and eddies from the open ocean; not shown). Northward transport across the 200-m isobath section is balanced by the sum of transports across the 100-m isobath section and through the cross-shelf section. The intrusive transport across the 200-m isobath is non-zero throughout the year, but it peaks during winter and is minimum in summer; their difference (i.e., winter minus summer) ranges from 0.18 to 0.3 Sv. This difference is of the same order as that found in Guo et al.'s (2006) model with more realistic topography and forcing. About half of the intrusive flux continues northward onto the shallow shelf (green curve, across the 100-m isobath), and another half (purple curve) turns east/northeastward between the 100 and 200-m isobaths. Both these fluxes also show seasonal variations:
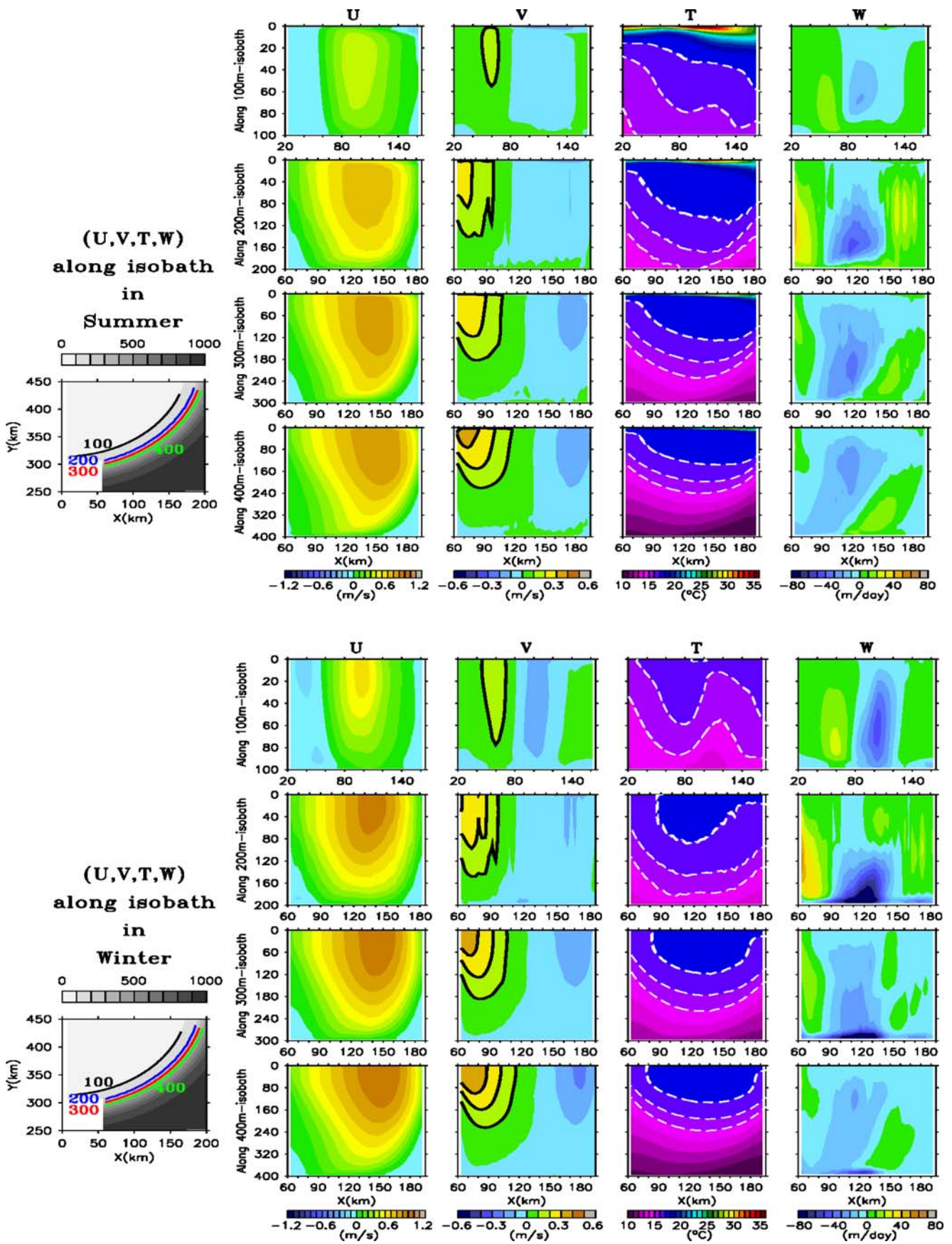
◄ **Fig. 6** Vertical section contours of along (U; >0 away from coast) and across (V; >0 towards the shallow shelf) isobath velocities, temperature T, and vertical velocity W along the 100, 200, 300, and 400-m isobaths for summer (*upper set of panels*) and winter (*lower set*). *Solid lines on* "V" are positive contours with minimum = 0.1 ms^{-1} at 0.1 ms^{-1} increment; *white dashed lines on* "T" are the 15, 16, and 17°C contours. *Insets on left* show isobaths and the same x coordinate in kilometer used in the sectional contour plots
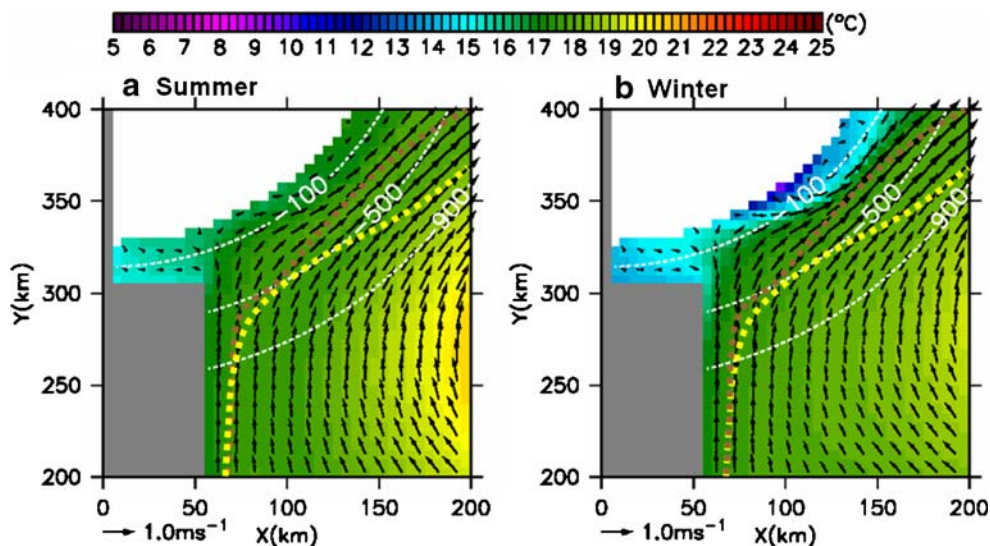
stronger transport in winter and weaker in summer, but the winter minus summer difference across the 100-m isobath is more prominent. The total intrusive transport (blue curve in Fig. 9a) is entrained back across the shelf break further downstream into the Kuroshio. We calculate that approximately 0.4 Sv is returned near the surface (see Fig. 5), and the remaining 0.15~0.4 Sv is downwelled into the lower layer and transported off-slope. An estimate of this latter off-slope flux is plotted in Fig. 9b as $\iint w(x, y, z = -30m).dxdy$ integrated over the outer shelf. This downwelling flux is least in summer, about −0.1 to −0.15 Sv. Therefore, most of the off-slope flux in summer is near the surface. The downwelling flux is largest in winter, as high as −0.45 Sv, and correlates well with the intrusive influx across the 200-m isobaths (Fig. 9a). The magnitude of this downwelling flux in winter agrees well with the intrusive transport across the 100-m isobaths (compare black (Fig. 9b) and green (Fig. 9a) curves), showing that cooling indeed accounts for the increased northward intrusion of the Kuroshio into the East China Sea.

The enhanced onshore intrusion in winter is now examined in term of depth-integrated vorticity balance. We noted in Fig. 6 that the lower layer motions are significant, and moreover, that the along isobath isotherms show bowl-shape structures; therefore the JEBAR effect can be important. The main balance in the depth-integrated vorticity equation is between $(Hu_a).\nabla(f/H)$ and $J(\chi, H^{-1})$, and

these are shown in Fig. 10 (note that $-J(\chi, H^{-1})$ is plotted). Other terms in Eq. 7 are 2~3 orders of magnitude smaller (not shown). It is seen that over the shelf and slope off the northeastern Taiwan, advection of geostrophic potential vorticity, $(Hu_a).\nabla(f/H)$, is large and positive, and it is balanced by the JEBAR term. The maximum magnitudes occur just after the Kuroshio crosses the $f/H= 20 \times 10^{-8} m^{-1} s^{-1}$ contour (or $H \approx 500$-m isobath) off the northeastern coast of Taiwan. The JEBAR is of the same sign and has similar structures both in summer and winter. Thus, irrespective of the season, the upper layer of the Kuroshio tends to deepen eastward along the (zonal running) isobaths northeast of Taiwan. However, it is clear that the winter maximum in $(Hu_a).\nabla(f/H)$ is larger than the corresponding summer maximum, indicating a stronger onshore intrusion in winter. It is also clear that the difference is caused, in winter, by a steeper offshore tilt of the isotherms, which accounts for the stronger JEBAR. The locations of these maxima coincide well with the locations where the Kuroshio begins to veer offshore (i.e., after crossing the 500-m isobath) as described previously. It is important to note that these differences between "summer" and "winter" are purely caused by the differential heat flux we have applied for the two seasons. Since wind and other forcing are nil, they cannot contribute to the differences. Finally, further north along the northeastward-curving isobaths (x>130 km) the JEBAR term changes sign ($J(\chi, H^{-1})$<0) consistent with an offshore veering of the model Kuroshio as noted previously in Fig. 6.

To complete the analysis, Fig. 11 shows the time series of area-averaged "$(Hu_a).\nabla(f/H)$" for the last 4 years of the model integration; this is nearly identical to the JEBAR time series which is omitted. The averaging region is between the $f/H=20 \times 10^{-8} m^{-1} s^{-1}$ and $100 \times 10^{-8} m^{-1} s^{-1}$ contours and also from 60 km<×<100 km as shown in the inset (the

Fig. 7 Color maps of temperatures at $z=-50$ m for **a** summer and **b** winter. Vectors are (u, v) at the same level. *Thick dotted lines* are Kuroshio paths in winter (*brown*) and summer (*yellow*)—see text. *Dotted white lines* are isobaths in meters
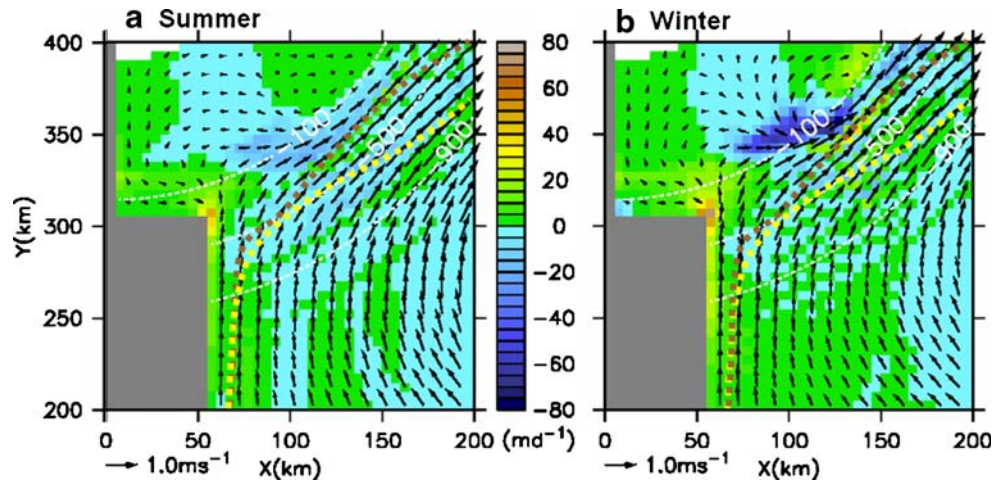
hatched region). The value of "$(Hu_a).\nabla(f/H)$" (and JEBAR) is positive indicating on-shelf intrusion of Kuroshio year round, and it is largest in winter and weak in summer, though the variation is not cyclical suggesting a highly nonlinear response. When converted into transports, the difference between winter and summer shelfward intrusive transports are about 0.2~0.3 Sv. Not surprisingly, the variation in Fig. 11 and the winter minus summer difference are very similar to those shown in Fig. 9.

Various model sensitivity tests were conducted to confirm the above result that cooling alone can account

for the on-shore migration of the Kuroshio off the northeastern coast of Taiwan during winter. Amongst the more important ones, in addition to the grid resolution experiments (mentioned previously), we experimented with (all using the same horizontal grid sizes = 5 km and 50 vertical sigma levels) (1) zero heat flux (i.e., no winter and summer difference), (2) different stratifications in the initial temperature field (Eq. 6): stronger and weaker, (3) slightly gentler slope: 100 m-1,000 m over a width of about 100 km instead of 50 km, and (4) reduced heat flux magnitude = 5×10^{-5}K m/s. The zero heat flux experiment "(1)" yields no

Fig. 9 **a** Ninety-day running
averaged volume transports
across the three indicated
sections (*left inset*) during
the 4-year analysis
period—"SUM" for summer
and "WIN" for winter. *Blue*
across the 200-m isobath
(>0 northward, mean = 0.63 Sv),
green across the 100-m
isobaths (>0 northward,
mean = 0.32 Sv); and *purple*:
across a cross-shelf section
between the 100 and 200-m
isobaths (>0 eastward,
mean = 0.31 Sv). *Thin colored
lines* indicate means.
b Thirty-day, running-averaged
downwelling volume flux
$\int\int w(x, y, z = -30\ m).dxdy$
over the red-shaded region on
the outer shelf (50 m<H<
150 m; *right inset*), also for the
4-year analysis period
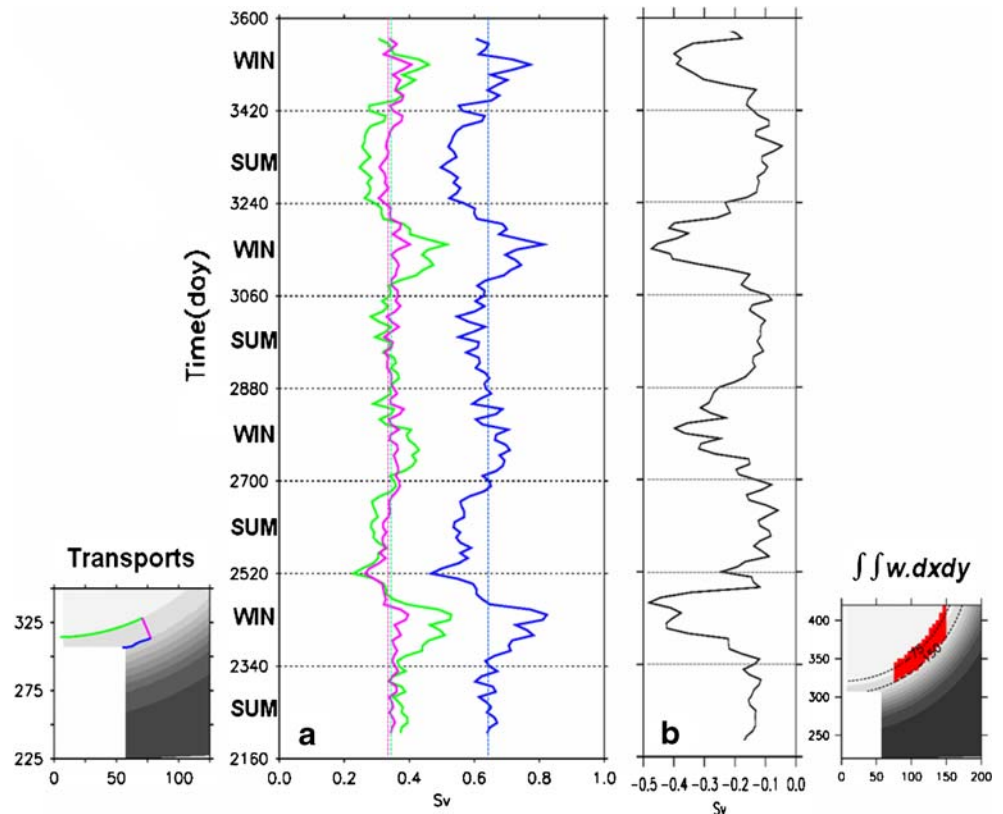
Fig. 10 The two dominant terms in the vorticity balance of the depth-averaged flow: advection of the geostrophic potential vorticity $(Hu_a).\nabla(f/H)$ (*left column* denoted CPVF) and the JEBAR term $-J(\chi, H^{-1})$; (*right column* denoted CJBAR), for **a** summer and **b** winter. *Contours* indicate values of "f/H" in unit of $10^{-8} m^{-1} s^{-1}$
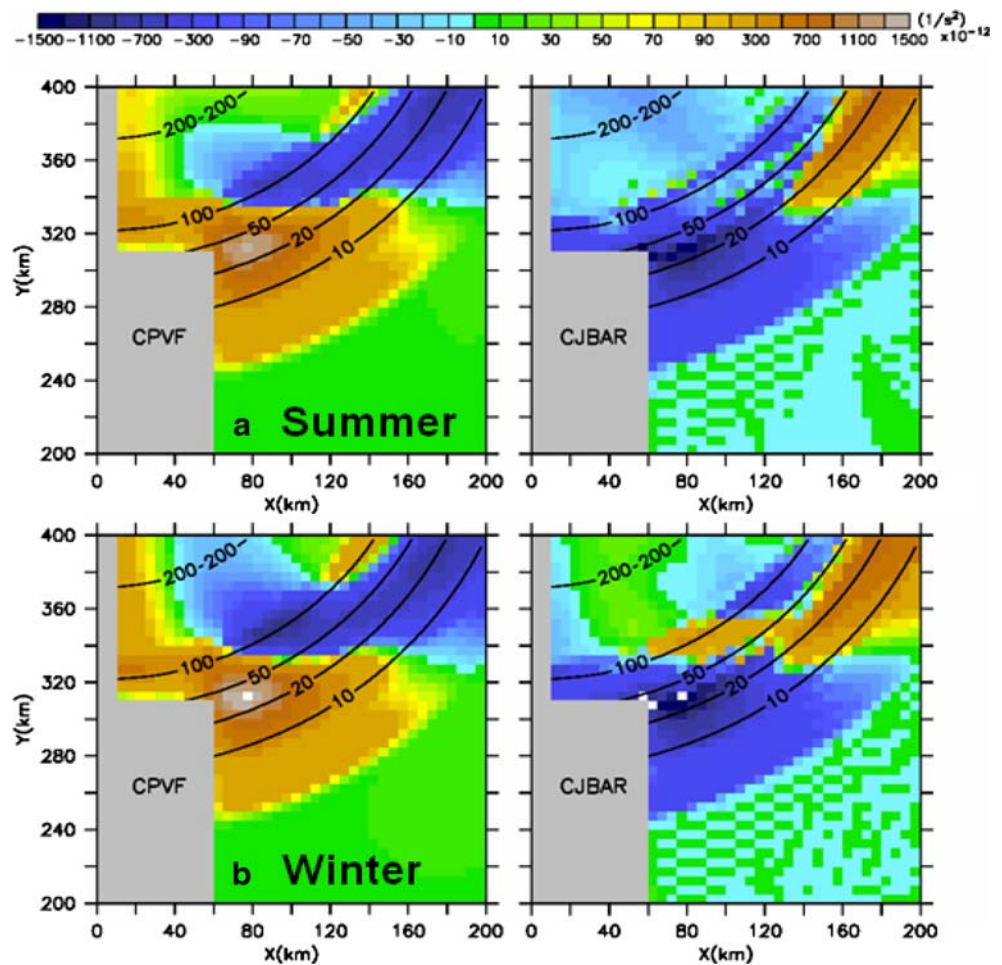
seasonal variation (as to be expected). The seasonal migration is not overly sensitive to the different initial stratifications we have chosen "(2)", nor to the slope value "(3)." The reduced heat flux experiment "(4)" yields a smaller migration.

## 5 Summary, discussion, and conclusion

The seasonal migration of Kuroshio across the shelf break of the East China Sea off the northeastern coast of Taiwan is examined based on the hypothesis that surface heat flux alone can explain the variability. The hypothesis is based on Tang and Yang's (1993) and Chuang and Liang's (1994) observations. These indicate that the timing of on-shelf intrusions coincides with the beginning of the cooling season (around September), and that moreover the on-shelf currents were not correlated with the wind.

To isolate the effect of cooling, we construct an idealized model consisting of three ingredients: a northward-flowing western boundary current (the Kuroshio) along Taiwan, a (nearly) zonal shelf and slope topography off Taiwan, and a winter surface heat loss that is strongest near Taiwan (and the

East China Sea) but that diminishes eastward. Unlike previous modeling studies (e.g., Chao 1991; Chen et al. 1996), the Kuroshio in the present case is spun up from the Sverdrup transport forced by wind stress curl over a closed basin, thus eliminating the need to specify open-boundary inflow and outflow. Moreover, wind and associated Ekman pumping are nil over the region of interest (i.e., shelf and slope). The seasonal differences in the model response are therefore caused purely by the inhomogeneity in the surface heat flux we impose.

The model results show a seasonal on-shelf intrusive response that is stronger in winter than in summer. The largest response is near the surface (upper 50~100 m) which agrees with Hsueh et al.'s (1992) description from observations that "… a part of the Kuroshio … penetrated northward as a shallow surface current." Stern and Austin (1995) show that the intruded water is entrained back into the western boundary current by downslope flow whose stretching provides the necessary cyclonic vorticity in an "inertial boundary layer," thus maintaining the current. We show that, in winter, cooling leads to enhanced downwelling of outer-shelf waters which cross-off slope; hence, also increased entrainment by the Kuroshio. This increased outflux is compensated by an
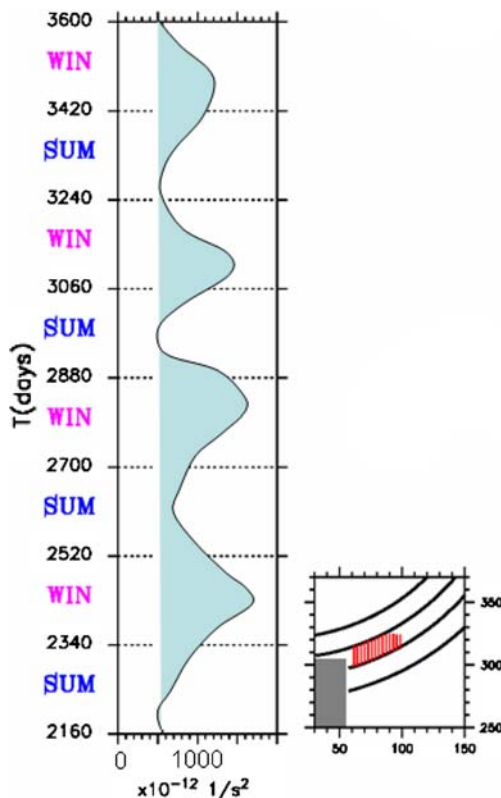
Fig. 11 Time series of area-averaged "$(Hu_a).\nabla(f/H)$" for the last 4 years of the model integration. The area-averaging region is hatched in the *lower right inset*. The time-series has been smoothed using a 120-day running average

enhanced intrusion of Kuroshio waters northeast of Taiwan. The downwelling velocity is increased by more than five times in winter compared to summer and it also produces increased stretching and stronger cyclonic vorticity. As a result, the inertial boundary layer is thinner in winter, since a fluid parcel can gain the required vorticity to maintain the current through stretching of isotherms due to downwelling, and need only to traverse less off-slope. All in all, shelfward intrusion of the Kuroshio northeast of Taiwan increases, and the current shifts closer to the outer shelf in winter.

The model results indicate that lower layer flow is not negligible. The effects of winter cooling are further examined through an analysis of the vorticity balance of the depth-averaged flows. This shows that the stronger on-shelf, cross-isobath intrusion in winter is accounted for by the JEBAR term. The stronger JEBAR arises because of the stronger along-isobath (i.e., approximately zonal) upper layer depth change (i.e., density gradient) induced in winter by stronger cooling near Taiwan than further offshore.

Appendix: two-layer planetary geostrophic model

The following two-layer (subscripts 1 and 2; hydrostatic) planetary geostrophic equations (include cooling and heating) are from Salmon (1992):

$$-fv_1 = -\partial\phi_s/\partial x - ru_1 \tag{1a}$$

$$+fu_1 = -\partial\phi_s/\partial y - rv_1 \tag{1b}$$

$$\partial h_1/\partial t + \partial(u_1 h_1)/\partial x + \partial(v_1 h_1)/\partial y = +Q \tag{1c}$$

$$-fv_2 = -\partial\phi_s/\partial x + g'\partial h_1/\partial x - ru_2 \tag{2a}$$

$$+fu_2 = -\partial\phi_s/\partial y + g'\partial h_1/\partial y - rv_2 \tag{2b}$$

$$\partial h_2/\partial t + \partial(u_2 h_2)/\partial x + \partial(v_2 h_2)/\partial y = -Q \tag{2c}$$

Here, ϕ_s is the surface pressure, r is the coefficient of Rayleigh friction, Q is cooling if negative modeled by a loss of mass from the upper layer (depth h_1) to the lower layer (depth h_2),

$$h_1 + h_2 = H(x,y) \tag{3}$$

is the total water depth, $g' = g(\rho_2 - \rho_1)/\rho_o$ is the reduced gravity, f = Coriolis parameter, and (u_i, v_i), i=1 or 2 is the velocity in the ith-layer. Our goal is to reduce the above set of equations to just two equations (Eqs. 8 and 11 or 12 below) involving only the upper layer depth h_1 and the stream function ψ for the total transport (define below). The forms of the equations follow those used by Isobe (2000). Eliminate ϕ_s [Eq. 1a − Eq. 2a and also Eq. 1b − Eq. 2b]:

$$+f(u_1 - u_2) = -g'\partial h_1/\partial y - r(v_1 - v_2) \tag{4a}$$

$$-f(v_1 - v_2) = -g'\partial h_1/\partial x - r(u_1 - u_2) \tag{4b}$$

The sum of Eq. 1c and Eq. 2c gives:

$$\partial(u_1 h_1 + u_2 h_2)/\partial x + \partial(v_1 h_1 + v_2 h_2)/\partial y = 0 \tag{5}$$

so that a (total) transport stream function $\psi(x, y, t)$ may be defined:

$$\partial\psi/\partial x = v_1 h_1 + v_2 h_2, \qquad -\partial\psi/\partial y = u_1 h_1 + u_2 h_2 \tag{6}$$

Together with Eq. 3, this Eq. 6 allows (u_2, v_2) to be written entirely in terms of (u_1, v_1), h_1, ψ and H. The resulting (u_2, v_2) is then substituted into Eq. 4 to yield $(u_1,$

v_1) in terms of h_1, ψ, and H. Finally, Eq. 6 then also yields (u_2, v_2) in terms of h_1, ψ, and H. Thus:

$$u_1 = -\psi_y/H - g'h_2h_{1y}/(fH) - g'\mathrm{r}h_2h_{1x}/(f^2H) \qquad (7\mathrm{a})$$

$$v_1 = +\psi_x/H + g'h_2h_{1x}/(fH) - g'\mathrm{r}h_2h_{1y}/(f^2H) \qquad (7\mathrm{b})$$

$$u_2 = -\psi_y/H + g'h_1h_{1y}/(fH) + g'\mathrm{r}h_1h_{1x}/(f^2H) \qquad (7\mathrm{c})$$

$$v_2 = +\psi_x/H - g'h_1h_{1x}/(fH) + g'\mathrm{r}h_1h_{1y}/(f^2H) \qquad (7\mathrm{d})$$

[To retain a symmetrical-looking set of equations, we have kept in Eqs. 7a, 7b the coefficient h_2/H; but of course this is just $(1-h_1/H)$]. Substituting Eq. 7 into Eq. 1c) gives:

$$\partial h_1/\partial t + (-\psi_y/H)(\partial h_1/\partial x) + (\psi_x/H)(\partial h_1/\partial_y) = \qquad (8)$$
$$\nabla \cdot (rR_o^2 \nabla h_1) + Q + (h_1/H)$$
$$\left[\left(-\psi_y/H\right) + g'h_1h_{1y}/(fH)\right]H_x + (h_1/H)$$
$$[(+\psi_x/H) - g'h_1h_{1x}/(fH)]H_y$$

where,

$$R_o^2 = g'h_1h_2/(f^2H) \qquad (9)$$

is the squared Rossby radius. We now vertical-average the x-momentum equation, thus $[h_1 \times \text{Eq. 1a} + h_2 \times \text{Eq. 2a}]/H$, giving:

$$-(f/H)(\partial\psi/\partial x) = -\partial\phi_s/\partial x + g'h_2h_{1x}/H + (r/H)(\partial\psi/\partial y) \qquad (10\mathrm{a})$$

Similarly, $[h_1 \times \text{Eq. 1b} + h_2 \times \text{Eq. 2b}]/H$ gives:

$$-(f/H)(\partial\psi/\partial y) = -\partial\phi_s/\partial y + g'h_2h_{1y}/H - (r/H)(\partial\psi/\partial x) \qquad (10\mathrm{b})$$

Taking the curl of Eq. 10, i.e., $[\partial(\text{Eq. 10b})/\partial x - \partial(\text{Eq. 10a})/\partial y]$, and using $h_2 = H-h_1$, gives:

$$-\psi_x \partial(f/H)/\partial y + \psi_y \partial(f/H)/\partial x - g'h_1h_{1x}H_y/H^2$$
$$+ g'h_1h_{1y}H_x/H^2$$
$$= \nabla \cdot [(r/H)\nabla\psi] \qquad (11)$$

This is the vorticity equation of the depth-averaged velocity. For our purpose, it suffices to take $f = $ constant, so that Eq. 11 becomes:

$$[\psi_x f - g'h_1h_{1x}]H_y + \left[-\psi_y f + g'h_1h_{1y}\right]H_x$$
$$= H^2\nabla \cdot [(r/H)\nabla\psi], \ f = \text{constant}. \qquad (12)$$

The vorticity balance Eq. 11 or Eq. 12 does not have an explicit time-dependent term because the momentum equations are steady in the planetary geostrophic model.

References

Allen JS, Newberger PA (1996) Downwelling circulation on the Oregon continental shelf, part I: response to idealized forcing. J Phys Oceanogr 26:2011–2035

Berntsen J, Oey LY (2010) Estimation of the internal pressure gradient in sigma-coordinate ocean models. Ocean Dynamics. doi:10.1007/s10236-009-0245-y

Carnevale GF, Smith SGL, Crisciani F, Purini R, Serravall R (1999) Bifurcation of a coastal current at an escarpment. J Phys Oceanogr 29:969–985

Chao SY (1991) Circulation of the East China Sea, a numerical study. J Oceanogr 42:273–295

Chen CTA (1996) The Kuroshio intermediate water is the major source of nutrients on the East China Sea continental shelf. Oceanol Acta 19:523–527

Chen HT, Yan XH, Shaw PT, Zheng QN (1996) A numerical simulation of wind stress and topographic effects on the Kuroshio current path near Taiwan. J Phys Oceanogr 26:1769–1802

Chuang WS, Liang WD (1994) Seasonal variability of intrusion of the Kuroshio water across the continental shelf northeast of Taiwan. J Oceanogr 50:531–542

Gong GC, Shiah FK, Liu KK, Chuang WS, Chang J (1997) Effect of Kuroshio intrusion on the chlorophyll distribution in the southern East China Sea north of Taiwan during Spring, 1993. Cont Shelf Res 17:79–94

Guo X, Miyazawa Y, Yamagata T (2006) The Kuroshio onshore intrusion along the shelf break of the East China Sea: the origin of the Tsushima warm current. J Phys Oceanogr 36:2205–2231

Hsueh Y, Wang J, Chern CS (1992) The intrusion of the Kuroshio across the continental shelf northeast of Taiwan. J Geophys Res 97:14323–14330

Huthnance JM (1984) Slope currents and "JEBAR". J Phys Oceanogr 14:795–810

Isobe A (2000) Two-layer model on the branching of the Kuroshio southwest of Kyushu, Japan. J Phys Oceanogr 30:2461–2476

Johns WE, Lee TN, Zhang D, Zantopp R, Liu CT, Yang Y (2001) The Kuroshio east of Taiwan: moored transport observations from WOCE PCM-1 array. J Phys Oceanogr 31:1031–1053

Liang WD, Tang TY, Yang YJ, Ko MT, Chuang WS (2003) Upper ocean currents around Taiwan. Deep-Sea Res Part II 50:1085–1105

Liu KK, Gong GC, Lin S, Yang CY, Wei CL, Pai SC, Wu CK (1992) The year-round upwelling at the shelf break near the northern tip of Taiwan as evidenced by chemical hydrography. Terres Atmos Ocean Sci 3:243–276

Mellor GL (2002) User's guide for a three-dimensional, primitive equation, numerical ocean model. Program in Atmospheric and Oceanic Sciences Report, Princeton University pp. 41

Mellor GL, Oey LY, Ezer T (1998) Sigma coordinate pressure gradient errors and the seamount problem. J Atmos Ocean Technol 15:1122–1131

Nitani H (1972) Beginning of the Kuroshio. In Kuroshio—its physical aspects, edited by H Stommel and K Yoshida, Unversity of Tokyo Press 129–163

Orszag SA (1971) Numerical simulation of incompressible flows within simple boundaries: accuracy. J Fluid Mech 49:75–112

Qu T, Mitsudera H, Yamagata T (1998) On the western boundary currents in the Philippine Sea. J Geophys Res 103:7537–7548

Salmon R (1992) A two-layer gulf stream over a continental slope. J Mar Res 50:341–365

Smagorinsky J (1963) General circulation experiments with the primitive equations: I the basic experiment. Mon Weather Rev 91:99–164

Stern ME, Austin J (1995) Entrainment of shelf water by a bifurcating continental boundary current. J PhysOceanogr 25:3118–3131

Sun X (1987) Analysis of the surface path of the Kuroshio in the East China Sea, in essays on investigation of Kuroshio, edited by X. Sun. China Ocean Press, Beijing, pp 1–14

Tang TY, Yang YJ (1993) Low frequency current variability on the shelf break northeast of Taiwan. J Oceanogr 49:193–210. doi:10.1007/BF02237288

Tang TY, Tai JH, Yang YJ (2000) The flow pattern north of Taiwan and migration of the Kuroshio. Cont Shelf Res 20:349–371

Wu CR, Lu HF, Chao SY (2008) A numerical study on the formation of upwelling off northeast Taiwan. J Geophys Res 113:C08025. doi:10.1029/2007JC004697

Wyrtki K (1961) Physical oceanography of the southeast Asian waters, scientific results of marine investigation of the South China Sea and the Gulf of Thailand. NAGA Report, vol 2. Scripps Inst Oceanogr, La Jolla, p 195

Zhang D, Lee TN, Johns WE, Liu CT, Zantopp R (2001) The Kuroshio east of Taiwan: modes of variability and relationship to interior ocean mesoscale eddies. J Phys Oceanogr 31:1054–1074